Final Report

DIFFERENCE IN SOURCE CHARACTERISATION BETWEEN SHALLOW AND DEEP FAULTING

External Grant Award Number: **06HQGR0043**

Arben Pitarka
URS Group, Inc.
566 El Dorado St., 2nd Floor
Pasadena, CA 91101-2560
626-449-7650
arben_pitarka@urscorp.com

Key words: Rupture Dynamics, strong-ground motion

1. INTRODUCTION

The characterization of kinematic fault rupture models that are currently used in numerical techniques for ground motion prediction is not fully constrained by physical rupture conditions. This leads to a crude representation of the observed ground motion variability caused by the complexities in the fault rupture process. One important observation that needs to be accommodated by the rupture models used in strong ground motion simulations is the difference in ground motion characteristics between buried and surface-rupturing earthquakes (Somerville, 2003; Kagawa et al., 2004). In general surface-rupturing earthquakes generate weaker near-fault ground motion than buried earthquakes. This difference is significant in the period range of 0.3-3 sec. One of the factors that may cause this phenomenon is the effect of the weak shallow layer (upper 5 km of the crust) on rupture dynamics during earthquakes (Day and Ely, 2002; Pitarka et al., 2005). This article presents results of our investigation of the weak shallow layer effect on rupture dynamics and near-fault ground motion from buried rupturing (asperity located below the weak zone) and surface rupturing (asperity located within the weak zone) during strike-slip earthquakes.

1.1 Observed Differences Between Shallow and Deep Faulting

As shown in Figure 1, at short and intermediate periods (0.3-3.0s) the recorded ground motions from earthquakes that produce large surface rupture are systematically weaker than the ground motions from earthquakes whose rupture is confined to the subsurface (Somerville, 2003). In particular, the recent Turkey and Taiwan earthquakes have surprisingly weak ground motion in the period range 0.1-2.0 sec, about 40% weaker than those of empirical ground motion models. Figure 2 shows these effects. In this figure the event terms for a set of surface rupture earthquakes are shown at the top, and for a set of subsurface rupture earthquakes at the bottom. The unit line represents the Abrahamson and Silva (1977) ground motion empirical model, and lines above the unit line indicate that the event's ground motions on average exceed the model.

The ground motions of buried rupture earthquakes are systematically stronger than these of the surface rupturing earthquakes over a wide period range. This phenomenon is not region dependent, since the recorded data used in the analyses are from crustal earthquakes in different regions around the world (Kagawa et al., 2004).

When analyzing the kinematic rupture models of several earthquakes, Kagawa et al.(2004) found that earthquakes with surface rupture have asperities (regions of large slip) at depths shallower than 5 km, while earthquakes with buried rupture have asperities that mostly are deeper than 5 km. Also compared with shallow asperities, deep asperities have on average three times larger stress drop as well as two times larger peak slip velocity. Although limited to long periods, kinematic rupture models of past earthquakes give a clear indication that the cause of the observed differences in ground motion amplitude and frequency content produced by surface and buried rupture is mainly due to differences in fault rupture dynamics in the shallow and middle regions of the crust. Large earthquakes consume more fracture energy as the rupture propagates along the shallow weak layer compared with confined deep rupture.

2. SHALLOW WEAK LAYER

Brune and Anooshehpoor (1998) described the physical properties of the weak layer and its effect in reducing high-frequency seismic energy during shallow faulting. The weak layer is a layer of relatively incompetent fault gouge that is not able to maintain large shear strain during earthquakes (e.g., Marone, 1998). During rupture the resisting force of the weak material increases with the slip velocity. This so-called velocity strengthening tends to reduce the particle velocity and rupture speed. As pointed out by Day and Ely (2002) the weak layer can also result from thick surface deposits of sediments with relatively low velocity. Low velocity materials are less capable of maintaining large strain energy. During rupture they may absorb high frequency waves, and amplify lower frequency waves, thus enhancing the effects of the weak fault zone on near-fault ground motion.

The presence of velocity strengthening friction at shallow depths has been observed in laboratory experiments where the rock friction at low normal stress exhibits velocity strengthening behavior (e.g. Marone et al., 1991; Marone, 1998; Shimamoto and Logan, 1981). Also studies of interseismic shallow creep (e.g. Lyons et al., 2002), and shallow post seismic slip of large earthquakes (Marone et al., 1991; Marone 1998) provide indirect evidence for a velocity strengthening fault rheology at shallow depths. Moreover, analyses of scaling properties of fracture energy derived from dynamic rupture models of past earthquakes (Mai et al., 2006) show that the fracture energy scales differently for surface rupture than it does for buried rupture. Their study suggests that surface-rupturing earthquakes consume more fracture energy as the rupture expands and reaches the free surface compared with buried rupture earthquakes.

Scale-model earthquake experiments using foam rubber blocks performed in laboratory by Brune and Anooshepoor (1998) provided compelling evidence of significant effects of a shallow weak layer on fault ground motion from strike-slip ruptures. Their experimental results suggested that shallow weak crustal layers may reduce the amplitude of high frequency energy generated during earthquakes. The interpretation of their experimental results supports two fundamental hypotheses about the cause of reduced high frequency radiation during shallow ruptures: 1) because of the weak material properties in the upper few kilometers, the fault zone may not be able to maintain high levels of shear strain required for high seismic energy release

during earthquakes, and 2) the velocity strengthening during rupture in the weak fault zone suppresses high frequency seismic radiation.

Day and Ely (2002) extended the original experimental investigation of Brune and Anooshepoor (1998) to studying the effects of the weak zone on near-fault ground motion. Using a 3D finite difference technique they demonstrated that the foam rubber experiment can be very well reproduced by rupture dynamic modeling using the slip weakening friction law combined with equivalent slip strengthening in the weak zone. Through numerical modeling they analyzed the propagation of rupture through the weak zone in more detail than is available from the laboratory observations alone. The numerical simulations predicted that the weak zone diminishes surface accelerations and velocities out to a fault-normal distance that scales with the weak-zone depth. Beyond this distance opposing effects on peak acceleration and peak velocity are observed. This suggests that the depth of the asperity during earthquake rupture controls the frequency content of the ground motion. This intriguing result provides insights into finding physical explanations of the difference in ground motion between buried rupturing and surface rupturing.

Pitarka et al., (2005) and Somerville and Pitarka (2006) used the results from these studies and numerical simulations of rupture dynamics to explain the frequency-dependent difference between observed ground motion from buried and surface rupturing. Their modeling of rupture dynamics using simple models with depth dependent frictional properties suggested a direct link between the significant changes in the rupture dynamics as it propagates through deep and shallow asperities, and the frequency content of the generated ground motion. However their exploratory study was based on a limited number of numerical experiments and simple homogeneous stress models.

In a more rigorous study Dalguer et al. (2008) proposed another explanation. They attributed the difference in ground motion between the two types of faulting to the differences in stress drop and hypocenter location. They infer that the surface-rupturing earthquakes are characterized by a large area of negative stress drop surrounding the asperities and a shallow hypocenter, while buried earthquakes are characterized by non-negative stress drop and a relative deep hypocenter located below the asperity. According to their model the buried faulting generates stronger high frequency ground motion mainly due to the upward directivity effect and higher stress drop. While surface faulting generates weaker high frequency ground motion because of the enhanced energy absorption due to large area of negative stress drop. In essence the calibrated dynamic rupture models of Dalguer et al. (2008) and the shallow weak-layer model (e.g., Day and Ely, 2002; Somervile and Pitarka, 2006) are similar since both assume large enhanced energy absorption areas of negative stress drop. They differ only in the location of such areas; in the shallow-weak layer model the negative stress drop area is mainly concentrated within the weak zone in the upper 5km of the crust.

In this study we pursue the concept of shallow weak layer effect on rupture dynamics to explain the observed difference in ground motion between surface and buried rupturing. We improved our original rupture dynamic simulations by using rupture models with stochastic stress drop and extended the analyses to faults with different lengths.

3. RUPTURE MODEL PARAMETERIZATION

In developing stochastic stress drop rupture models we followed the work of Andrews (1980), Day (1982), and Oglesby and Day (2002). The fundamental assumption in Andrews model is that the stress drop is scale invariant i.e. earthquakes of different sizes have the same stress drop. We adopted a stochastic characterization of the spatial complexity of earthquake rupture stress drop in which the stress distribution is described by a power spectral density function in the wave number domain, parameterized by two characteristic length scales, along the strike and dip directions (e.g., Somerville et al., 1999). The spectral decay above the corner wave number along the strike and dip directions is proportional to K^{-1} where K is the wave number (Andrews, 1980). The spectral decay controls the roughness of the spatial stress distribution. In terms of ground motion K^{-1} spectral stress model is equivalent to the K^{-2} spectral slip model. Both models produce w^2 type near-fault ground motion. Stochastic models described by a power density function have also been used for describing the kinematic slip distribution on the fault (e.g., Somerville et al., 1999; Mai and Beroza 2002; Lavalee and Archuleta, 2003; Liu et al., 2006) and initial stress (e.g., Ripperger et al., 2007). We assume that the stress drop depends on the regional stress whereas its small-scale fluctuations are caused by the variation of sliding friction on the fault. These spatial stress fluctuations are intended to represent the effect of fault surface random irregularities in generating high frequency ground motion.

Following Oglesby and Day (2002), both shear and normal stress in our models are considered variable, but they have the same spatial variation pattern. The key parameter is the relative fault strength which is measured as $S= (\sigma_y - \sigma_o)/ (\sigma_o - \sigma_f)$ where σ_y is yield stress, σ_o is initial stress, and σ_f is the sliding frictional stress. In the low-stress regions, which serve as barriers to the rupture, the relative fault strength is kept higher. In contrast, in the high-stress drop areas, which are prone to rupture, S is maintained low. Both conditions are satisfied by a small modification of the assumed initial spatial distribution of the normal stress σ_n^o following the technique of Oglesby and Day (2002):

$$\sigma_n = \sigma_n^o + \varepsilon (\max (\sigma_n^o) - \sigma_n^o)$$

where σ_n is the normal stress to be used in the dynamic model, σ_n^o is the initial random normal stress, and the maximum of σ_n^o is to be taken over the entire fault. The constant of proportionality ε for the added-in increment is used to control the roughness of the asperities. Finally the shear and normal stress distributions are scaled to produce a given average stress drop which is invariant in all rupture scenarios. We fixed ε at 0.01. This produces a rather rough stress drop distribution. Except for the weak zones for which we applied special conditions explained in subsequent sections, in all models the dynamic friction coefficient is 0.54 and Dc is 30 cm. The static friction coefficient was selected based on the condition that the average value of S should be greater than 2. Under this condition all generated models produced rupture speeds that remain subshear over large areas, except for very small regions where low S may have increased the rupture speed to supershear. The fault is a vertical plane embedded in a heterogeneous space with one horizontal surface layer. The velocity model is described in Table1.

In order to suppress the unrealistically large energy generated at the fault boundaries from externally imposed stopping behavior we applied velocity strengthening around the bottom and lateral fault boundaries. This approach is facilitated when using stress drop as the random field. The velocity strengthening below the seismogenic zone (depth greater than 15 km) was

introduced by linearly increasing the dynamic friction coefficient and the slip weakening displacement. In this area the stress drop linearly decreases to negative values. This parameterization produces a realistic rupture arrest and a rapid decrease of slip in the transition zone between the brittle frictional sliding and ductile rupture during the earthquake. The rupture nucleates at a given location in a rectangular area where the strength excess is forced to zero by adjusting the coefficient of static friction.

The spectral parameters of our finite source models include the average stress drop (scale invariant), fault strength factor S, and stress drop correlation lengths along strike and dip directions. The stress correlation lengths are determined based on Mw using the empirical relations of Somerville et al. (1999). Other empirical relations based on fault length and fault width can be used as well (e.g., Martin and Beroza, 2002). In simulations of rupture dynamics we used three different stochastic stress models for each of the four strike–slip earthquake scenarios with the magnitude Mw ranging from 6.9 to 7.3, and fault length L of 26km, 36km, 46km, and 56km, respectively. For the surface rupture scenarios the rupture depth range was restricted to 0-17.km, stress drop was 5 MPa, and hypocentral depth 7.5 km. For the buried rupture scenarios, the rupture depth range was 3-17km, stress drop was 7.5MPa and, hypocentral depth 10 km.

Figure 3 illustrates a stochastic stress model for a surface-rupturing earthquake on a 26 km long fault. Also shown in this figure are the depth variations of normal stress, stress drop and Dc, averaged along the strike of the fault. The station locations for the rupture scenarios considered in this study are presented in Figure 4. We used three linear arrays of stations located on the free surface. The linear arrays are parallel to the fault trace. Their fault distances (distance normal to the fault trace) are 2 km, 5 km, and 10 km, respectively.

4. SIMULATION OF WEAK ZONE EFFECTS ON RUPTURE DYNAMICS

The spontaneous rupture simulations were performed using a staggered grid finite difference code (Pitarka and Dalguer, 2003) that uses the traction-at-split-node method of Dalguer and Day (2006). The grid spacing is 150 m. We used the slip weakening friction law (e.g., Andrews, 1976; Day, 1982). This type of friction has been shown to work very well in modeling fault slip behavior inferred from seismic recordings of past earthquakes (Ide and Takeo, 1997; Olsen et al, 1997, Day et al, 1998; Dalguer et al., 2001, Ma et al., 2008) and has been demonstrated to produce equivalent results with the rate and state friction law (e.g., Kaneko et al. 2007; Bizzari and Cocco, 2005). The velocity strengthening in the weak layer was modeled using the slip weakening friction law with appropriate values of dynamic friction coefficient yielding depth varying negative stress drop (e.g. Day and Ely, 2002). The large area of apparent negative stress drop in the weak zone during rupture is supposed to reflect observed energy losses from the off–fault damage zone where energy is dissipated. In the weak layer the slip weakening distance increases linearly from 30 cm at the bottom of the layer to 100 cm at the free surface. The dynamic friction coefficient follows a linear decay that causes the stress drop to linearly decrease from around 5MPa at the bottom of the weak layer to negative values at the surface. A fast decrease in the stress drop results in a rupture arrest soon after the rupture enters the weak zone. We use this approach in developing buried rupture scenarios.

We started our investigation by simulating three M6.9 surface rupturing earthquakes, and one M6.9 buried rupture earthquake. Each earthquake is represented by three scenarios with

different stochastic stress drop distributions. The average stress drop for the surface rupture models was 5 MPa. For buried rupture models the average stress drop was 7.5MPa. The higher stress drop was chosen to compensate for the smaller rupture area of buried rupture scenarios (Kagawa et al., 2004) and match the seismic moment of surface rupture scenarios. The equivalent seismic moment allows for direct comparison of simulated ground motion among different scenarios.

Figure 5 shows examples of stochastic stress drop, and corresponding calculated slip and rupture time for models of surface rupture and buried rupture. The depth variations of averaged stress drop, slip-weakening distance and total slip are also shown. The four scenarios result in different slip variations with depth. The slip variation follows closely the variation of stress drop. It is obvious that the weaker the zone the smaller the shallow slip. Due to the upward rupture inertia and its interaction with the free surface, slip occurs even in weak areas of negative stress drop. A similar effect is also seen in the deep weak zone, located at depths between 15 and 20 km depth where the slip decreases to zero at a depth of 17.5 km,

The absence of a shallow weak layer causes the large asperity area to concentrate along the free surface. In this case the size of the asperity and slip increase dramatically. In contrast, the weak layer in the other two scenarios of surface rupture produces much smaller shallow slip. However the amount of slip in the weak zone remains significant even though the stress drop decreases to negative values.

Figure 6 shows the time history of the slip rate at receivers in a vertical array located on the fault. We show results corresponding to surface rupture with hypocenter located at 7.5 km depth, buried rupture with hypocenter located at 7.5 km, and buried rupture with hypocenter located at 10 km. Among the most interesting features of the simulated slip velocity two are relevant to our investigation of the frequency content of radiated seismic energy. First, the slip velocity of surface rupture weakens toward the surface and the effective rise time of slip in the weak zone becomes longer causing generation of weaker ground motion. In contrast, at the same locations, below the weak zone, the slip rate function of buried ruptures is sharper and has larger peak amplitude than that of surface rupture. The shorter effective rise time generates stronger high-frequency ground motion. The upward rupture directivity effect, manifested as increased slip rate amplitude toward the surface, is stronger by 30% for buried rupture compared to surface rupture. Second, the overall rupture directivity effect controlled by the large slip area and relative hypocenter location has a significant effect on the slip rate of buried rupture. The deeper hypocenter causes the large slip area to move deeper, creating conditions for stronger upward (shorter period) directivity effect and weaker lateral (longer period) directivity effect. As a result deep buried rupture earthquakes may generate stronger short period ground motion than shallow buried rupture earthquakes of the same seismic moment.

5. DIFFERENCE IN GROUND MOTION BETWEEN SURFACE AND BURIED RUPTURE

.

Somerville (2003) investigated the ground motion difference between surface and buried rupturing earthquakes by comparing the response spectral amplitude of individual earthquakes averaged over the recording sites with amplitude of the average earthquake as represented by the empirical model of Abrahamson and Silva (1997). For consistency with Somerville's comparisons we used a similar two-step procedure. First we computed the amplitude spectrum

for both types of rupture by averaging over three realizations of each scenario and over stations with same fault distance. Then, for each fault distance we computed the ratio between the average spectrum of buried rupture and average spectrum of surface rupture.

Figure 7 compares the spectral ratios between the buried rupture and surface rupture earthquakes. The surface rupture earthquakes were computed using models with high–gradient weak zone, low-gradient weak zone, and no weak zone, respectively. The ratios are calculated for fault-normal, fault-parallel and vertical components of ground motion velocity in the period range of 0.2-10 sec. As a general observation, the buried rupture ground motion is stronger on the fault normal direction only, as is seen comparing Figure 7a with Figure 7b and Figure 7c. For models with weak layer the fault-normal ground motion from buried rupture is higher than that of surface rupture in the period range of 0.7-4 sec and periods shorter than 0.3 sec at fault distances of 2 km and 5 km. Surface rupture models with low stress drop gradient in the weak zone produce larger ground motion in the period range 0.3-0.7 sec. This period range broadens to 0.3-2 sec at the fault distance of 10 km. The overall characteristics of the fault normal ground motion from surface rupturing earthquakes are affected by lateral rupture directivity, enhanced by shallow slip, and wave propagation effects of the low velocity surface layer.

As expected, the surface rupture scenario without weak layer produces very large surface slip. The resulting ground motion is unrealistically high, and much higher than that of buried rupture.

Mai et al, (2005) found that most earthquakes have hypocenters located in regions of large slip. This association implies that surface rupture, whose large slip region is often shallow, will nucleate at shallow depths, as opposed to buried rupture which is confined at larger depths. The effect of variation in hypocentral depth on buried/surface ratio is shown in Figure 8. In this figure we compare spectral ratios between buried ruptures initiated at depths of 7.5 km (thick line) and 10 km (thin line) and surface rupture for fault-normal and fault-parallel components of ground motion. The effect of the hypocentral depth is significant. Due to rupture directivity and weak zone effects the buried fault ground motion is in general high at period ranges 0.2-0.4 sec and 1-4 sec for short fault-distances of 2 and 5 km. The situation changes slightly at the fault distance of 10 km where both surface and buried ruptures produce similar ground motion in the intermediate period range (0.3-1sec). At this distance the ground motion is mainly affected by wave propagation, which is not sensitive to small variations in rupture initiation depth.

The simulation results we have shown so far are for comparisons between surface and buried rupture earthquakes with the same magnitude and same fault length. We performed simulations by adding our analyses by modeling surface-rupturing earthquakes with fault length of 26 km, 36 km, 46 km and 56km, respectively. Their corresponding magnitudes Mw are in the range 6.9-7.3 (Table 2). Figure 9 shows examples of distributions of slip and rupture time obtained for surface rupture earthquakes with different fault lengths. Note that all rupture realizations have the same hypocentral location, and have scale invariant average stress drop of 5 MPa. The fault and station configurations used in the calculation of near-fault ground motion are shown in Figure 4.

Table 2 summarizes the relation between seismic moment and slip for each scenario. There is a slight increase of peak slip with the fault length while the average slip and surface slip remain approximately the same for all considered magnitudes. These characteristics are compatible with the observed slip-length scaling of large earthquakes. As will be shown later, our modeling technique produces ground motion that saturates with magnitude, a distinctive trend manifested in empirical models of moderate size strikes-lip earthquakes. This desirable

feature is a consequence of the deep weak zone used in our dynamic rupture models that allows the development of coseismic slip with long rise time at depths below 15 km. The deep weak zone represents the brittle ductile transition at the base of the seismogenic zone (e.g. King and Wesnosky, 2007).

The simulated ground motion at near fault stations from surface rupturing of long faults is characterized by a large variation with D, distance along the fault away from the epicenter. This variation is caused by the cumulative effect of small-scale stress-drop heterogeneities along the rupture path, and rupture interaction with the free surface. Obviously, the averaging of buried/surface spectral ratio over all stations may inhibit spatially varying characteristics of interest. For this reason we calculated the average spectral ratio using stations with distance D covering three ranges, D< 20km, 20km<D<30km and D>30 km, respectively. The result for shallow and deep buried rupture initiations are shown in Figure 10. From this figure it is clear that for D shorter than 20 km the spectral ratio between buried and surface rupture is independent of the fault length.

At a fault distance of 2 km the deep buried rupture earthquakes produce stronger ground motion for periods up to 3 sec. In contrast they produce weaker ground motion at periods longer than 3 sec (Figure 10 a). The period range of larger amplitude narrows to about 1-3 sec for fault distances of 5km and 10 km. Also at these distances the ground motion from buried rupture earthquakes becomes weaker in the short period range of 0.3-0.7 sec. The ground motion amplitude from buried rupture increases when the hypocentral depth increases. It is obvious that the upward directivity in the buried rupture earthquakes plays a crucial role at producing larger ground motion at short and intermediate periods. These trends also remain noticeable in the D range between 20 km and 30 km (Figure 10 b).

For D greater than 30 km and considered fault distances the ground motion from surface rupturing earthquakes is larger than that of buried rupturing earthquakes (Figure 10 c). The variation of the ground motion characteristics as a function of D and fault length is illustrated in Figure 11. In this figure we show acceleration response spectra calculated at selected stations. Our numerical simulations predict that for small D and very near to the fault the ground motion from buried rupture is higher than that from surface rupture for all considered periods, independent of the fault length of surface rupture. The effect of fault length becomes important at larger D (over 30 km) and near-fault locations where the ground motion from surface rupture is higher at long periods, but still comparable with that of the buried rupture. Finally at 10 km from the fault the effect of the weak zone is small. The surface rupture ground motion from long faults becomes larger at all periods.

It can be argued that these features and the cut-off D of 30km are model related and strongly depend on the friction characteristics of the weak-zone and stress drop. The simulated ground motion from buried rupturing scenario earthquakes could be higher if the stress drop for these earthquakes was higher. In fact in our buried rupture models the average stress drop is only 50% higher than that of surface rupturing earthquakes. Nevertheless because the upward rupture directivity for buried ruptures, and lateral rupture directivity for surface ruptures affect different frequency bands, when the weak layer is present, the buried/surface amplitude difference near the fault can decrease with distance D. Using a simpler stress model Day and Ely (2002) found similar effects. Their numerical experiments suggest that at fault distances larger than the weak zone depth the effect of the weak zone is small.

6.CONCLUSIONS

The effect of the weak zone on rupture dynamics has already been established through foam-rubber laboratory experiments (Brune and Anooshehpoor, 1998) and numerical simulations (e.g., Day and Ely, 2002; Pitarka et al., 2005; Somerville and Pitarka, 2006; Kaneko et al., 2007). In this study we investigated the implications of a weak zone for near-fault ground motion amplitudes from strike-slip earthquakes in order to explain the observed difference in frequency content of ground motion between small, buried earthquakes, and large, surface-rupturing earthquakes.

Using numerical experiments with strike-slip earthquakes on faults with different lengths we found that a 5 km thick weak surface layer representing both a weak fault zone and shallow sedimentary deposits in the crust is capable of reducing the high frequency seismic radiation and increasing the rise time when friction in the weak zone is modeled as velocity strengthening. Our simulation suggests that large negative stress drop in shallow areas and increased slip weakening distance in the weak zone are required to correctly simulate both rupture arrest during buried rupture earthquakes and reduced slip velocity and longer rise time during surface rupturing large earthquake.

Our modeling results demonstrate that the combined effects of the weak layer and rupture directivity cause a significant contrast in frequency content of ground motion between buried and surface rupturing earthquakes. The confinement of large slip areas below the weak layer, and deep rupture initiation during buried earthquakes were found to be key factors in ground motion amplification in the period range 0.2-3 sec at sites very close to the fault. In contrast, as a result of the weak zone effect, the ground motion from shallow-slip surface rupturing earthquakes is greatly reduced in the same period range. These two opposing effects and higher stress drop due to smaller rupture area make the ground motion from small buried earthquakes larger than that from large surface rupturing earthquakes. The period range of this trend in ground motion differences is narrowed to 0.8-3 sec for fault distances of 5 km and longer.

Our simulation suggests that the difference in frequency content of ground motion from buried and surface rupture has limited spatial extent. The upward directivity effect during buried earthquakes is significant only in a narrow region above the asperity. This turns out to be the controlling factor of the spatial extent of the simulated contrast in frequency content between the two types of rupture. We found that at distances along the fault and away from epicenter that are smaller than 30 km, and fault distances smaller than 10 km the ground motion from small buried rupture earthquakes is larger than the ground motion from surface rupturing earthquakes. In general, beyond these distances the ground motion from surface rupturing earthquakes is larger. The cut-off distances found here are model dependent. They are related to the friction characteristics and width of the weak zone, and the assumed stress drop.

7. REFERENCES

Abrahamson, N.A. and W.J. Silva (1997). Empirical response spectral attenuation relations for shallow crustal earthquakes. *Seism.Res. Lett.* 68, 94-127.

Andrews, D.J. (1976). Rupture velocity of plane-strain shear cracks, *J.Geophys. Res.*, 81,5679-5687.

Andrews, D.J. (1980). A stochastic fault model , 1, Static case, *J.Geophys. Res.*, 78,3867-3877.

Bizzarri, A., and M. Cocco (2005). 3D dynamic simulations of spontaneous rupture propagation governed by different constitutive laws with rake rotation allowed. *Annals of Geophysics*, Vol. 48, N.2, 288-299.

Brune, J. N., and A. Anooshehpoor (1998). A physical model of the effect of a shallow weak layer on strong ground motion for strike-slip rup tures, *Bull. Seism. Soc. Am.* 88, 1070–1078.

Dalguer L.A, K. Irikura K, J. Riera and H.C. Chiu (2001). The importance of the dynamic source effects on strong ground motion during the 1999 Chi-Chi (Taiwan) earthquake: brief interpretation of the damage distribution on buildings, *Bull. Seism. Soc. Am.*, 95, 1112-1127.

Dalguer, L. A. and Day, S. M. (2007), Staggered-Grid Split Nodes Method for Spontaneous Rupture Simulation. *J. Geophys. Res.*, 112, B02302, doi:10.1029/2006JB004467

Dalguer, L.A., H. Miyake, S.M. Day, and K. Irikura (2008). Surface-rupturing and buried dynamic rupture models calibrated with statistical observations of past earthquakes, *Bull. Seism. Soc. Am,* 98 (in press)

Day, S. M. (1982). Three-dimensional simulation of spontaneous rupture: the effect of nonuniform prestress, *Bull. Seism. Soc. Am.*, 72, 1881-1902.

Day, S. M., and G. P. Ely (2002), Effect of a shallow weak zone on fault rupture: Numerical simulation of scale-model experiments, *Bull Seismol. Soc. Am.*, 92, 3006 – 3021.

Day, S. M., L. A. Dalguer, N. Lapusta, and Y. Liu (2005), Comparison of finite difference and boundary integral solutions to three-dimensional spontaneous rupture, *J. Geophys. Res.*, 110, B12307, doi : 10. 1029/ 2005JB003813.

Ide,S. and M. Takeo (1997). Determination of constitutive relations of fault slip based on seismic wave analyses. *J.Geophys. Res.* 102,27379-27391.

Kagawa, T., K. Irikura and P. Somerville (2004). Differences in ground motion and fault rupture process between surface and buried rupture earthquakes. *Earth, Planets and Space* 56,3-14.

Kaneko, Y., N. lapusta, J-P. Ampuero (2007). Spectral-element modeling of spontaneous earthquake rupture on rate and state faults: Effects of velocity-strengthening friction at shallow depths. *J. Geophys. Res.* (submitted).

Lavallee, D. and R. Archuleta (2003). Stochastic modeling of slip spatial complexities for the 1979 Imperial valley, California, earthquake. *Geophys. Res. Lett*, Vol. 30, No.5, 1245, doi:10.1029/2002GL015839.

Liu, P., R. Archuleta, and S. H. Hartzell (2006). Prediction of broadband ground motion time histories: frequency method with correlation random source parameters. *Bull. Seis. Soc. Am.*,96, 2118-2130, doi: 10.1785/0120060036.

Lyons, S. N., Y. Bock, and D. T. Sandwell (2002), Creep along the Imperial Fault, southern California, from GPS measurements, *J. Geophys. Res.*, 107, doi:10.1029/2001JB000763.

Ma., S., S. Custodio, R. Archuleta, and P. Liu (2008). Dynamic modeling of the 2004 Mw 6.0 Parkfield, California earthquake. *J. Geophys. Res.*, 113, B02301, doi:10.1029/ 2007JB005216.

Mai, P.M., and G.C. Beroza (2002). A spatial random field model to characterize complexity in earthquake slip, *J.Geophys. Res.*, 107(B11), 2308,doi:10.1029/2001JB000588.

Mai, P.M., P. Spudich, and J. Boatwright (2005). Hypocenter locations in finite-source rupture models, *Bull. Seis. Soc. Am.*, 95, 965-980.

Mai, P. M., P. Somerville, A. Pitarka, L. Dalguer, S. G. Song, G. Beroza, H. Miyake, and K.

Irikura (2006). On scaling of fracture energy and stress drop in dynamic rupture models: Consequences for near-source ground motions, in *Earthquakes: Radiated Energy and the Physics of Faulting*, R. Abercrombie, A. McGarr, H. Kanamori, and G. Di Toro, (Editors), AGU Geophysical Monograph Series 170, 283-293.

Marone, C.J., C. H. Scholz, and R. Bilham (1991), On the mechanics of earthquake afterslip, *J. Geophys. Res.*, 96, 8441- 8452.

Marone, C. (1998), Laboratory-derived friction laws and their application to seismic faulting, *Ann. Revs. Earth and Plan.Sci.*, 26,643-696.

Marone, C., and C. H. Scholz (1988). The depth of seismic faulting and the upper transition from stable to unstable slip regimes, *Geophys. Res. Lett.* 15, 621–624.

Oglesby, D. D., and S. M. Day (2003). Stochastic fault stress: implications for fault dynamics and ground motion, *Bull Seism. Soc. Am.* , 92, 3006-3021.

Olsen, K.B., R. Madariaga, and R. Archuleta (1997). Three dimensional dynamic simulation of the 1992 Landers earthquake, *Science*, 278,834-838.

Pitarka, A. (1999), 3D elastic finite-difference modeling of seismic motion using staggered grid with nonuniform spacing, *Bull. Seism. Soc. Am.*, 89, 54 – 68.

Pitarka, A. and L. Dalguer (2003). Estimation of dynamic stress parameters of the 1992 Landers earthquake (Abstract,AGU Fall Meeting, San Francisco).

Pitarka, A., S. Day, and L. Dalguer (2005). Investigation of shallow crustal weak zone effects on rupture dynamics of surface and subsurface faulting. *Proceedings and Abstracts Vol. XV, 2005 SCEC Annual Meeting, Palm Springs, California*, 168.

Rice, J.R; C G. Sammis, and R. Parsons (2005), Off-Fault Secondary Failure Induced by a Dynamic Slip Pulse, *Bull. Seism. Soc. Am.*, 95, 109 - 134.

Ripperger, J., P.M. Mai, and J.-P. Ampuero (2007). Variability of near-filed ground motion from dynamic earthquake rupture simulations.

Shimamoto, T., and J.M. Logan (1981). Effects of simulated clay gouges on the sliding behavior of Tennessee sandstone, *Tectonophysics*, 75,243-255.

Somerville, P.G. (2003). Magnitude scaling of the near fault rupture directivity pulse. Phys. Earth. Planetary. Int., 137, 201-212.

Somerville, P.G. and A. Pitarka (2006). Differences in earthquake source and ground motion characteristics between surface and buried earthquakes. *Proceedings of the Eighth National Conference on Earthquake Engineering, San Francisco, California.*

Somerville, P., K. Irikura, R. Graves, S. Sawada, D.J. Wald, N. Abrahmason, Y. Iwasaki, T. Kagawa, N. Smith, and A. Kowada (1999). Characterizing crustal earthquake slip models for the prediction of strong ground motion, *Seismological Research Letters*, 70 (1), 59-80

Table 1. Crustal Velocity Model

Layer	Vp (km/s)	Vs(km/s)	Density (g/cm^3)	Q
Sediments	4.8	2.8	2.4	200
Bedrock	6.0	3.46	2.67	1000

Table 2. Rupture Parameters of Buried Rupture and Surface Rupturing Scenario Earthquakes

Type of Rupture	Fault Length (km)	Mo (dyne cm)	Mw	Max. Slip (m)	Average Slip (m)	Stress Drop (MPa)
surface	26	2.94×10^{26}	6.9	4.4	2.4	5.0
surface	36	4.65×10^{26}	7.1	4.4	2.6	5.0
surface	46	6.35×10^{26}	7.2	4.7	2.8	5.0
surface	56	8.28×10^{26}	7.3	5.0	3.0	5.0

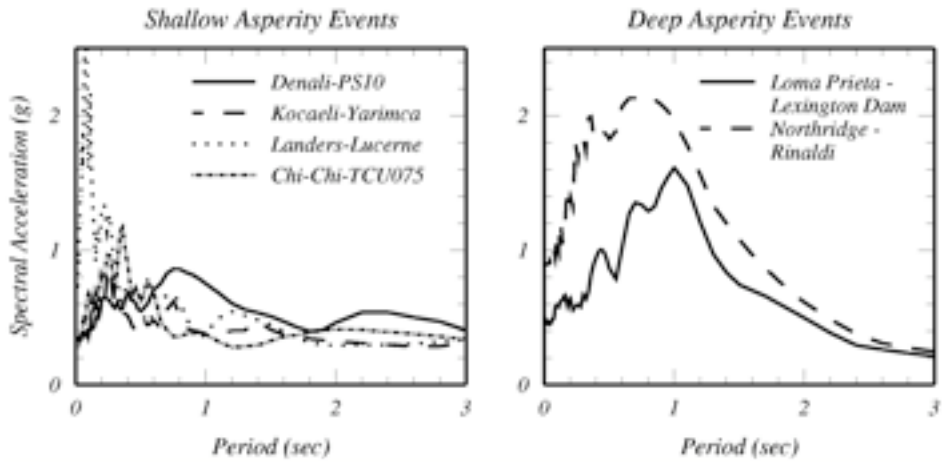

Figure 1. Near-fault response spectra of recent large earthquakes. Left: Four earthquakes, Mw 7.2 to 7.9, with shallow asperities and large surface faulting. Right: Two earthquakes, Mw 6.7 and 7.0, with deep asperities and no surface faulting. Source : Somerville and Pitarka (2006)

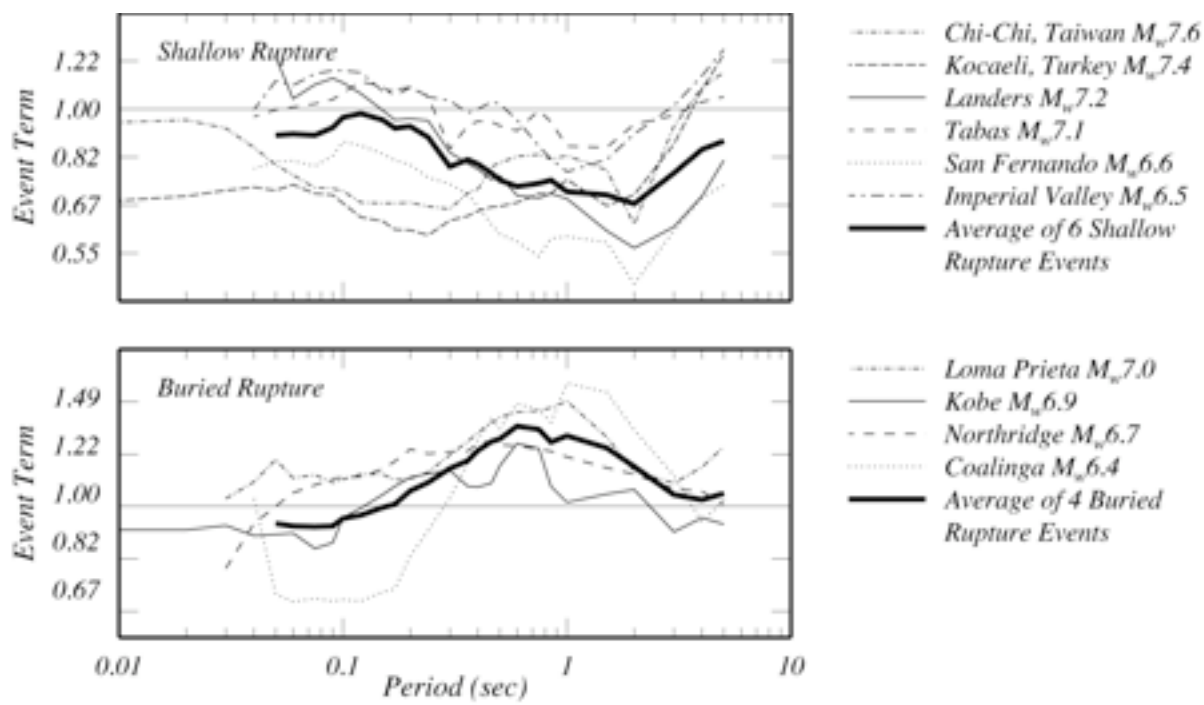

Figure 2. Comparison of response spectral amplitude of individual earthquakes having surface rupture (top) and buried rupture (bottom), averaged over recording sites, with the amplitude of the average earthquake as represented by the model of Abrahamson and Silva (1997), represented by the unit line, which accounts for magnitude, closest distance and recording site category. The event terms (residuals) are shown as the ratio of the event to the model. Source: Somerville (2003).

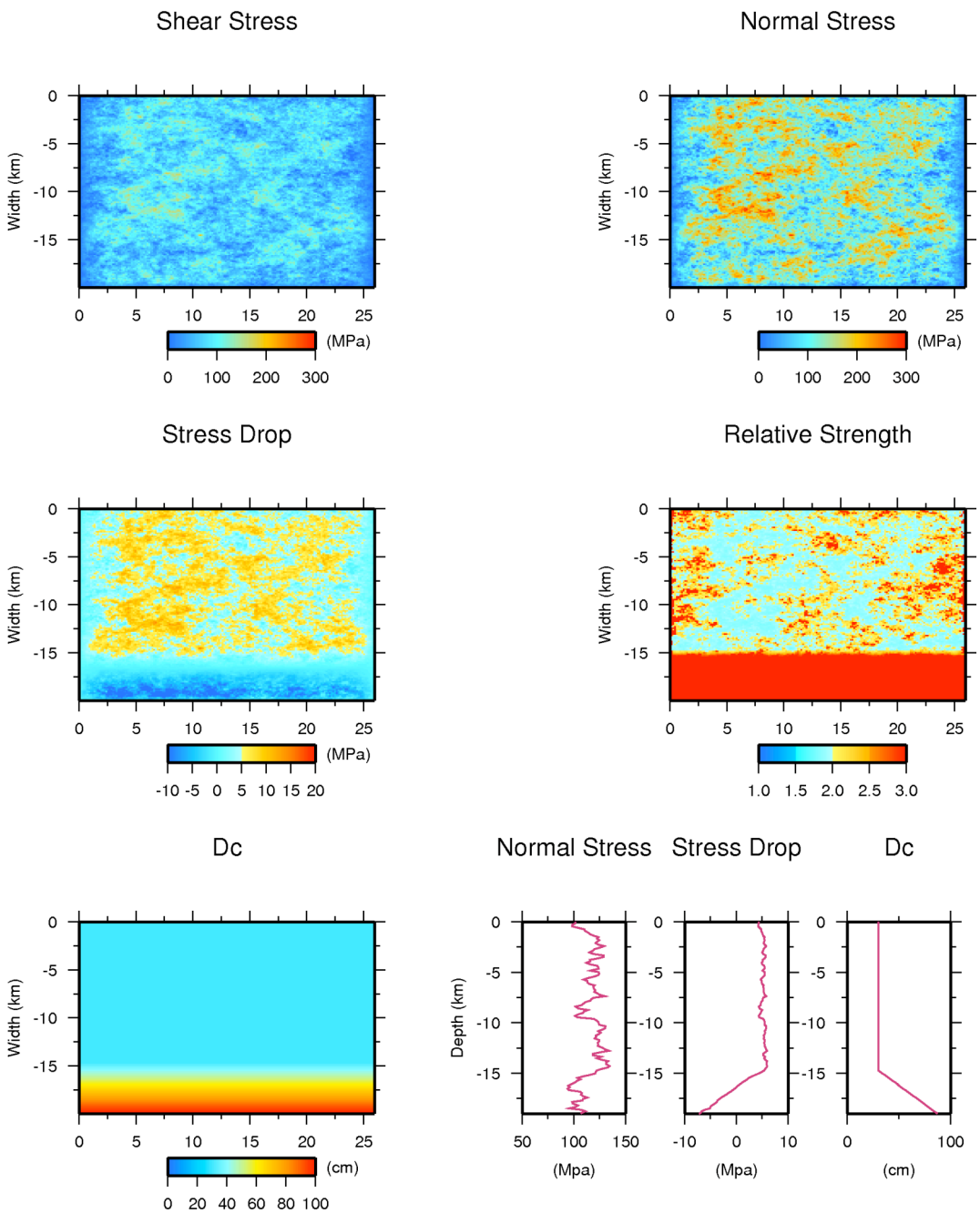

Figure 3. Stochastic stress model for a surface-rupturing earthquake on a 26 km long fault. Lowest panel show depth variation of normal stress, stress drop and slip weakening distance Dc, averaged along the strike of the fault. Note that we used a deep weak zone to simulate the rupture arrest at a depth of 17.5 km. The deep weak zone located at depths between 15 km and 20 km is modeled by a linearly decreasing stress drop, and linearly increasing Dc.

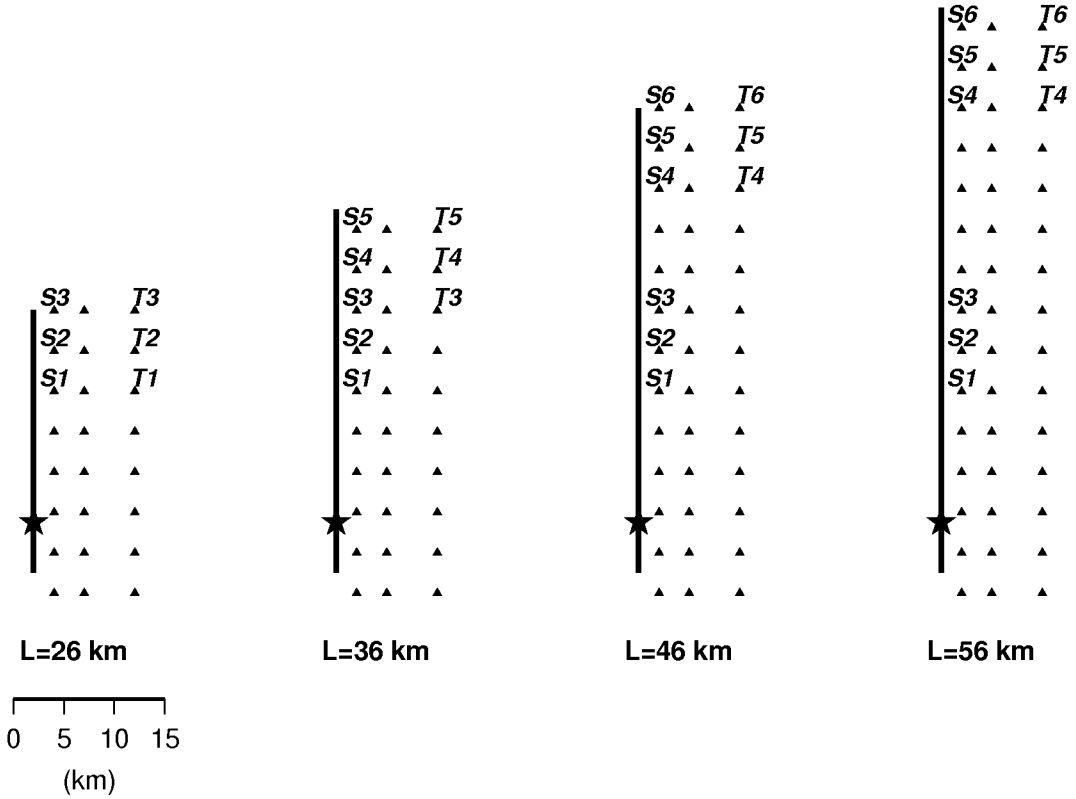

Figure 4. Fault-stations configurations considered in simulating rupture dynamics on vertical faults with different lengths. Triangles are stations and stars are epicenters. Selected stations whose ground motion is referred to in the text are given a name.

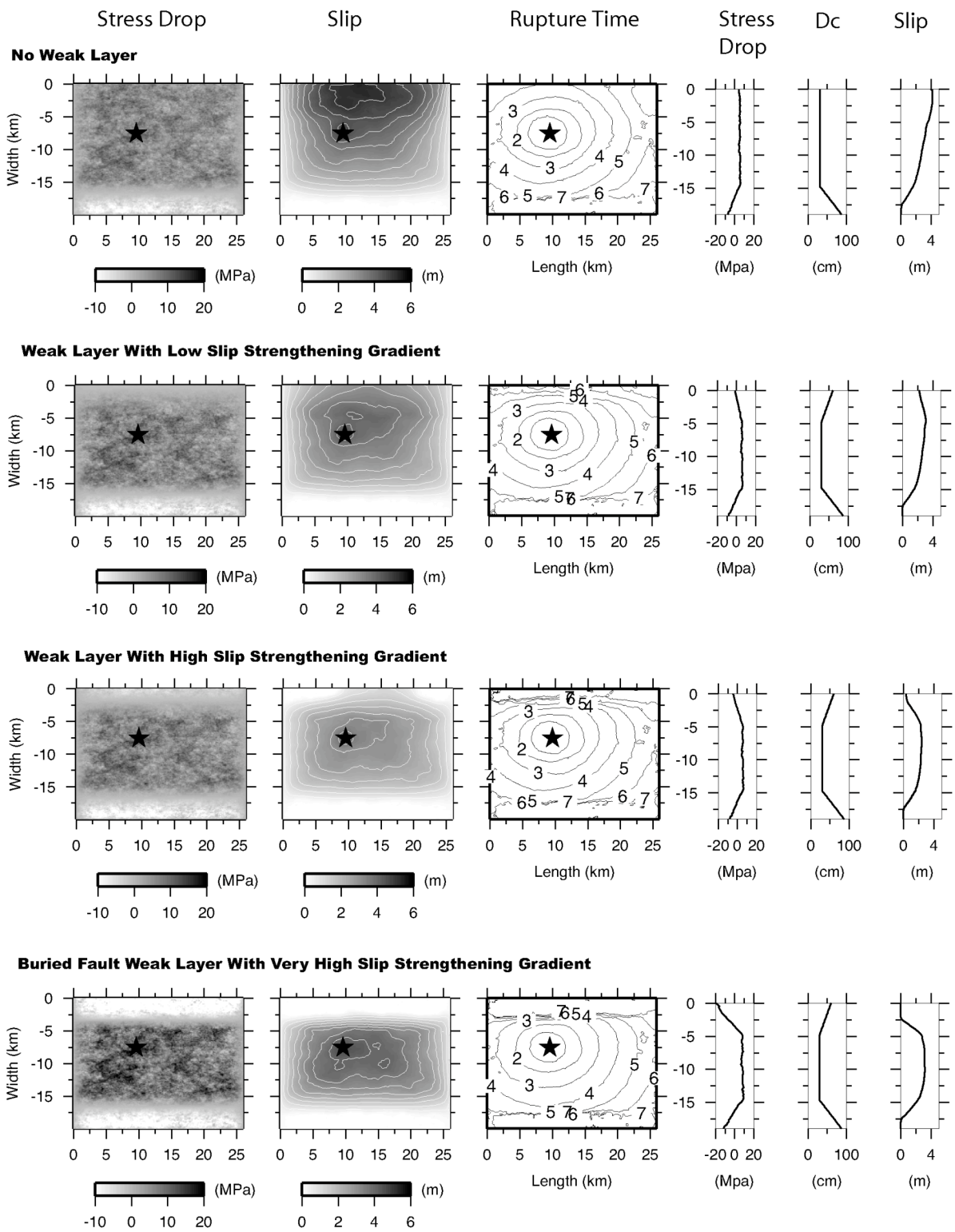

Figure 5. Examples of stochastic stress drop, and corresponding calculated slip and rupture time for models of surface rupture and buried rupture. The depth variations of averaged stress drop, slip-weakening distance and total slip are shown on the right. The four scenarios result in different slip variations with depth. The slip variation follows closely the variation of stress drop. Note that the weaker the zone (larger negative stress drop) the smallest the shallow slip.

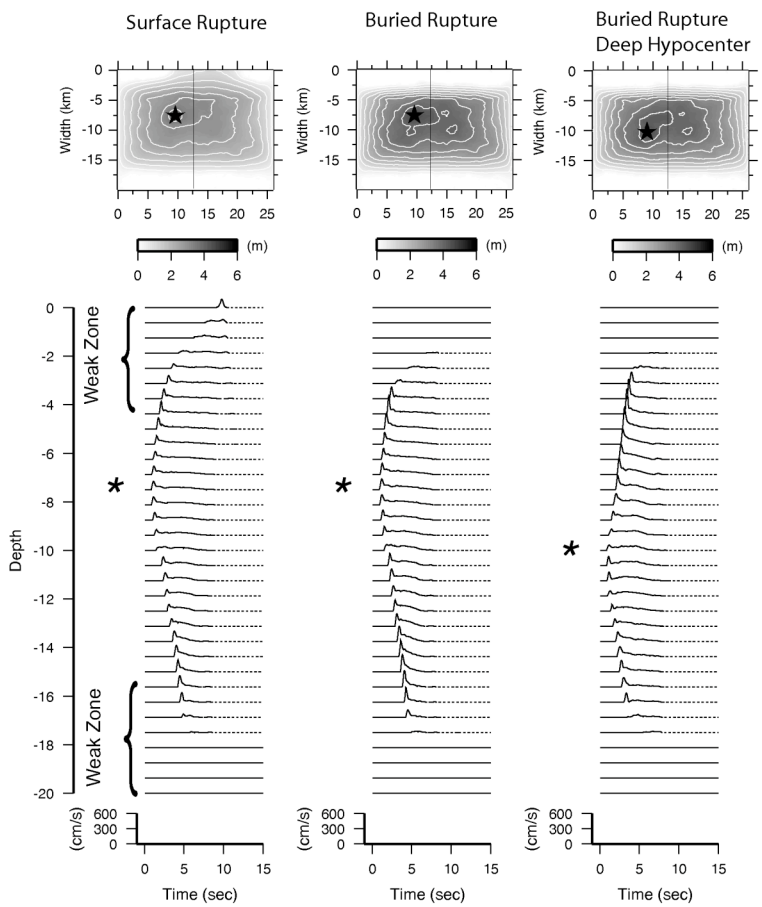

Figure 6. Time history of slip rate at receivers in vertical arrays located on the fault for surface rupturing (left panels), buried rupture with shallow epicenter (middle panels) and buried rupture with deep epicenter (right panels). Top panels show the corresponding slip distributions for each type of rupture. The vertical station arrays are indicated by solid lines on the slip distribution panels. Stars show epicenter locations. Note the considerable amplitude reduction of slip velocity in the shallow zone during surface rupturing, and larger peak slip velocity below the shallow weak zone during buried rupture with deep hypocenter.

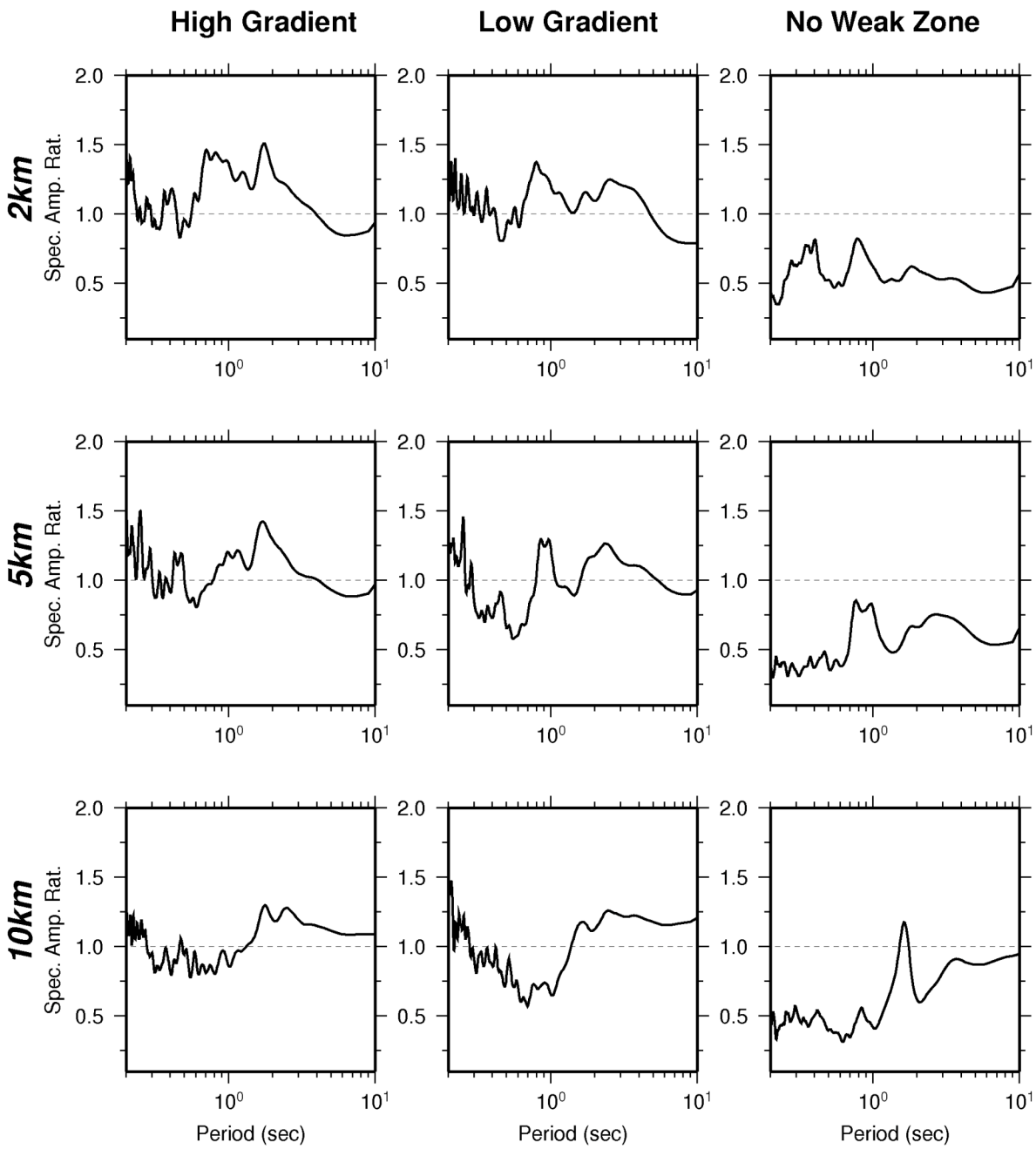

Figure 7a. Average spectral ratios of fault-normal ground motion velocity between buried rupture and surface rupturing earthquakes calculated at fault distances of 2 km (top panels), 5 km (middle panels), and 10 km (bottom panels). The ground motion for surface rupturing earthquakes was computed using stress models with high–gradient weak zone (left panels), low-gradient weak zone (central panels), and without weak zone (right panels), respectively.

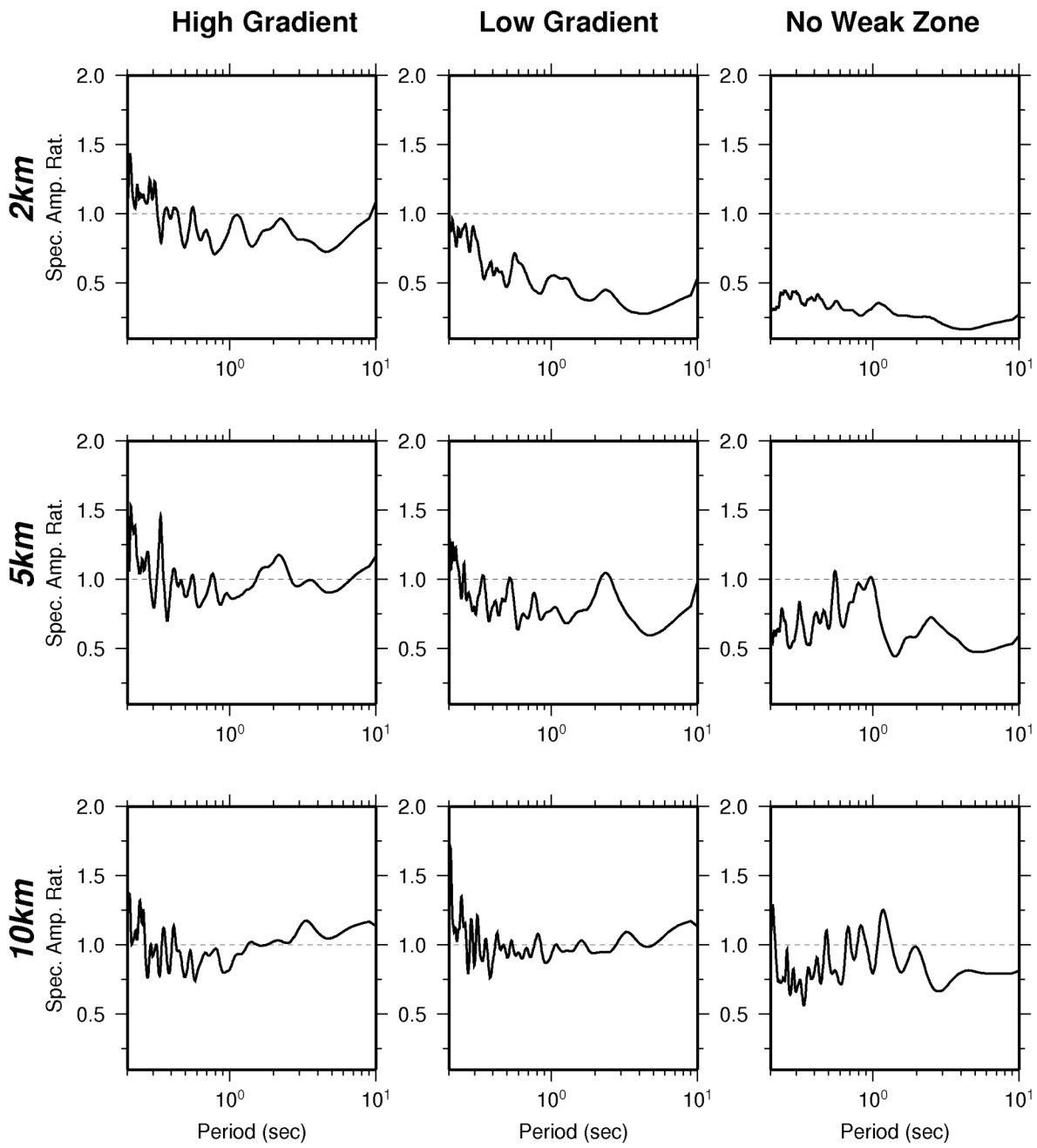

Figure 7b. Same as Figure 7a but for fault parallel component.

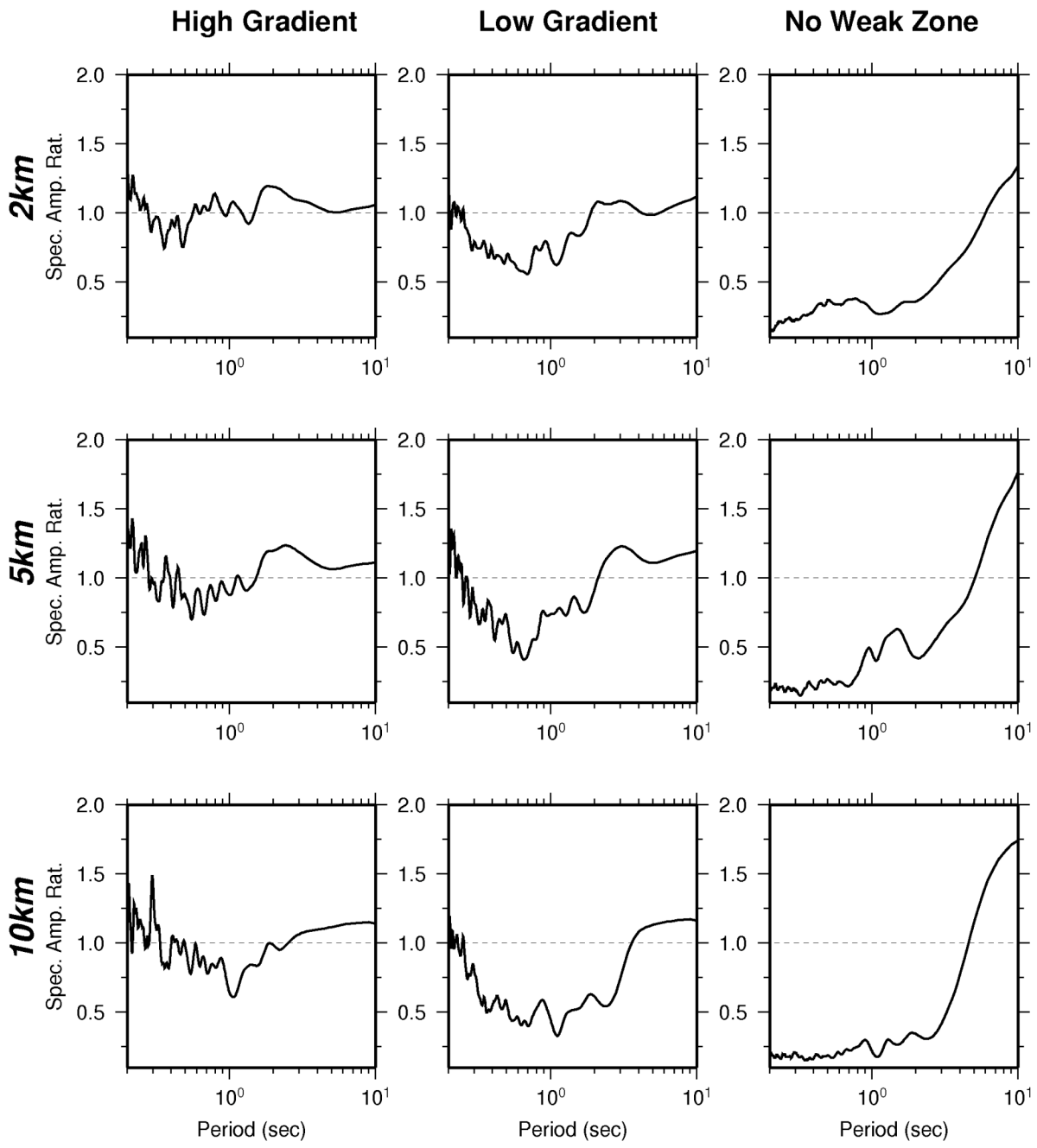

Figure 7c. Same as Figure 7a but for vertical component.

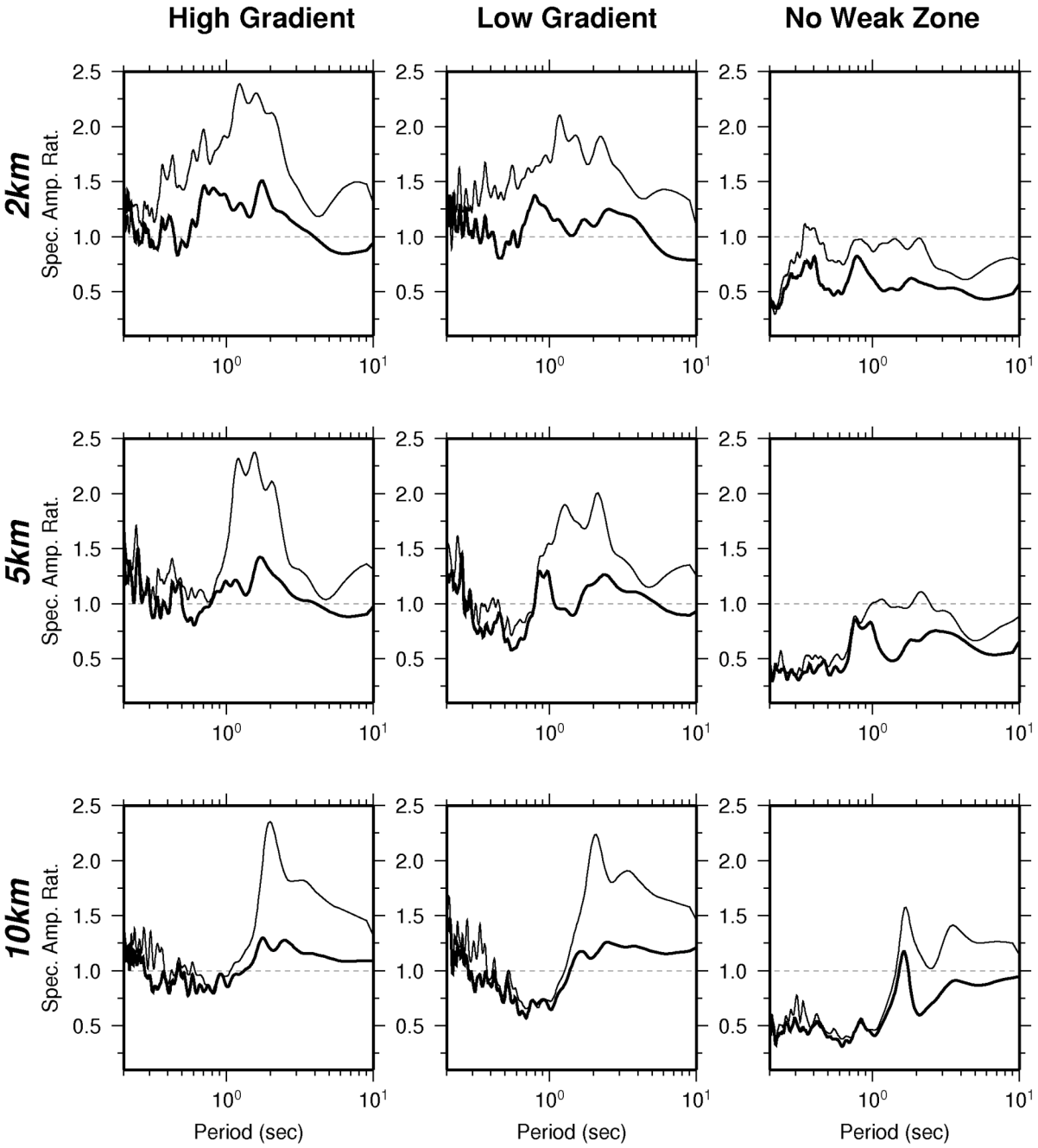

Figure 8a. Spectral ratios of fault normal ground motion velocity between buried rupturing earthquakes initiated at 7.5 km (thick line) and 10 km (thin line) depths and surface rupturing earthquakes calculated at fault distances of 2 km (top panels), 5 km (middle panels), and 10 km (bottom panels). The ground motion for surface rupturing earthquakes was computed using stress models with high–gradient weak zone (left panels), low-gradient weak zone (central panels), and no weak zone (right panels), respectively.

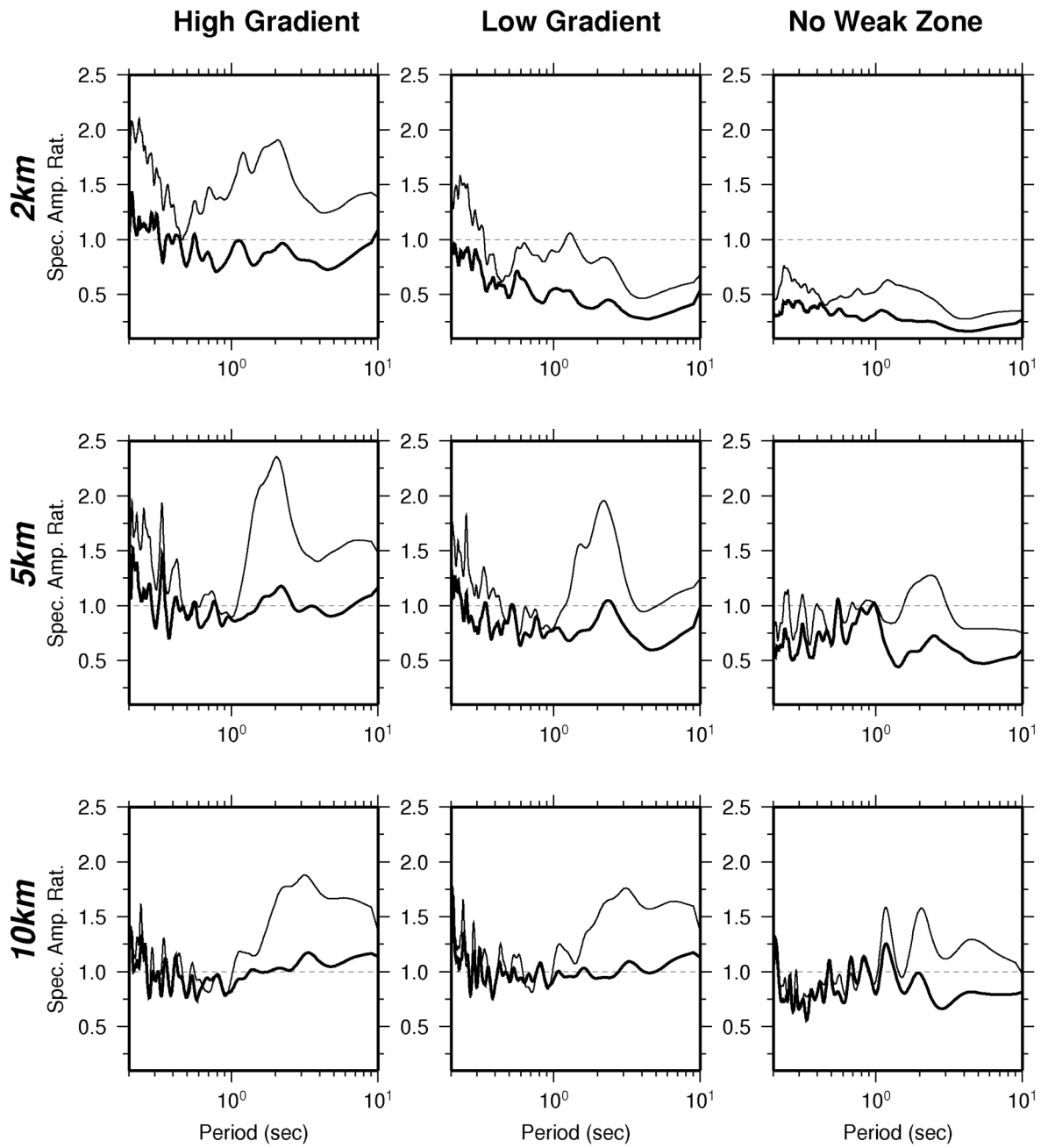

Figure 8b. Same as Figure 8a but for fault-parallel component.

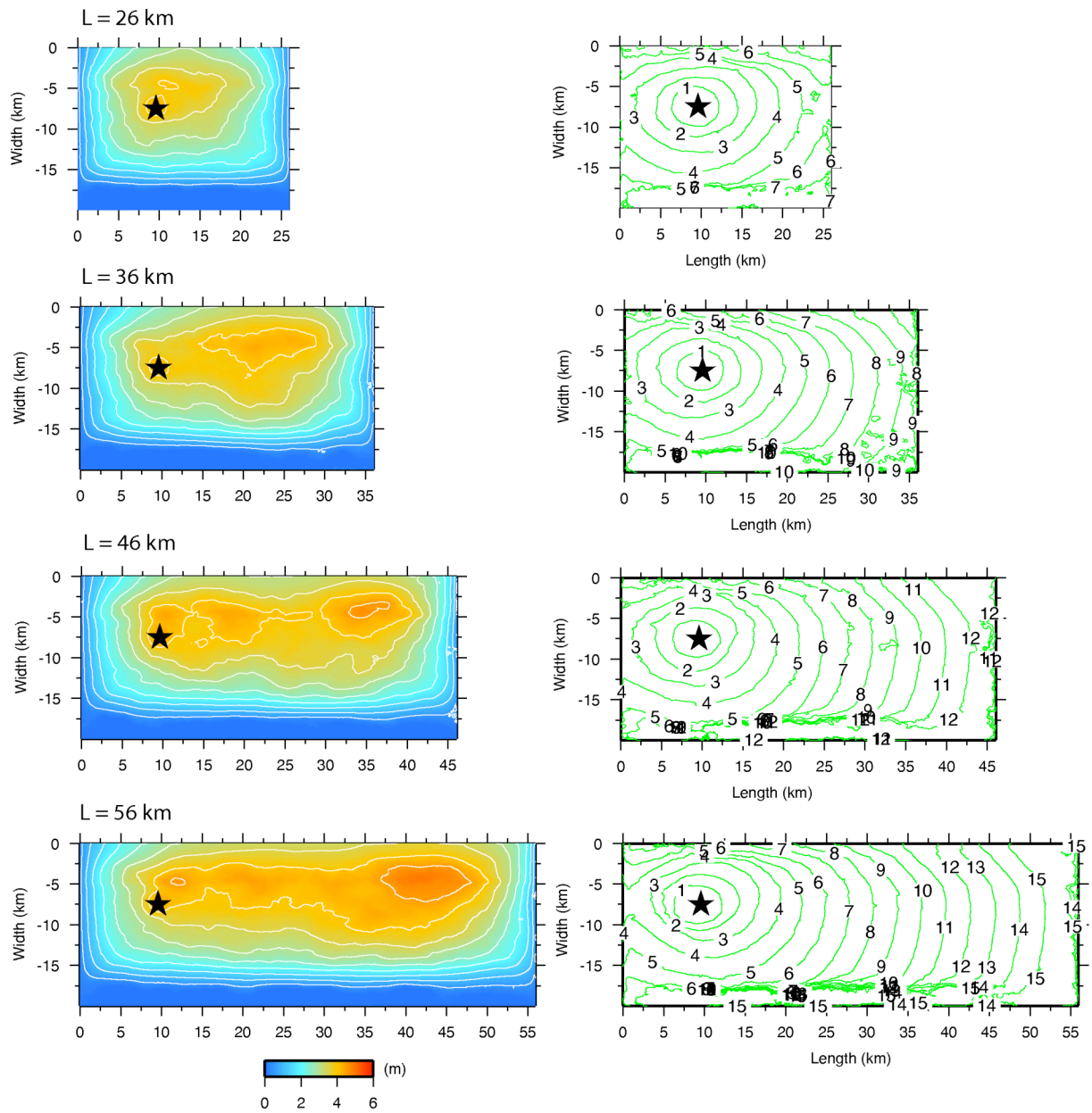

Figure 9. Selected distributions of slip and rupture time obtained for surface rupture earthquakes with different fault lengths L. L is indicated on top of each panel. Note that all rupture realizations have the same hypocentral location, and average stress drop of 5 MPa. Stars indicate the hypocenter location.

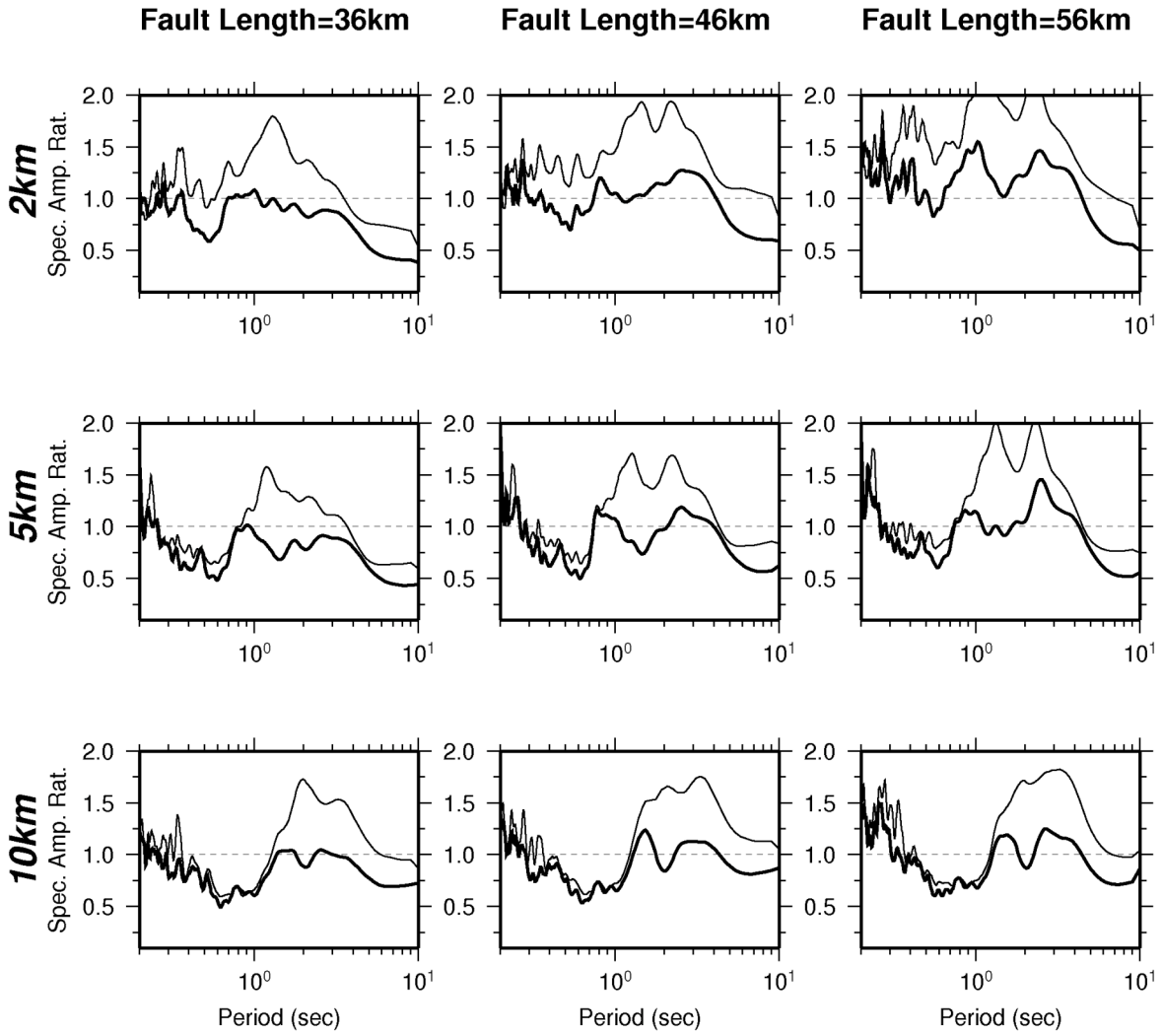

Figure 10a. Spectral ratios of fault-normal ground motion velocity between buried rupture earthquakes with 26 km fault length, and surface rupturing earthquakes with fault lengths of 36 km, 46 km, and 56 km, respectively, averaged over stations with D, distance along the fault away from the epicenter, less than 20 km. The buried rupture was initiated at 7.5 km depth (thick line) and 10 km depth (thin line).

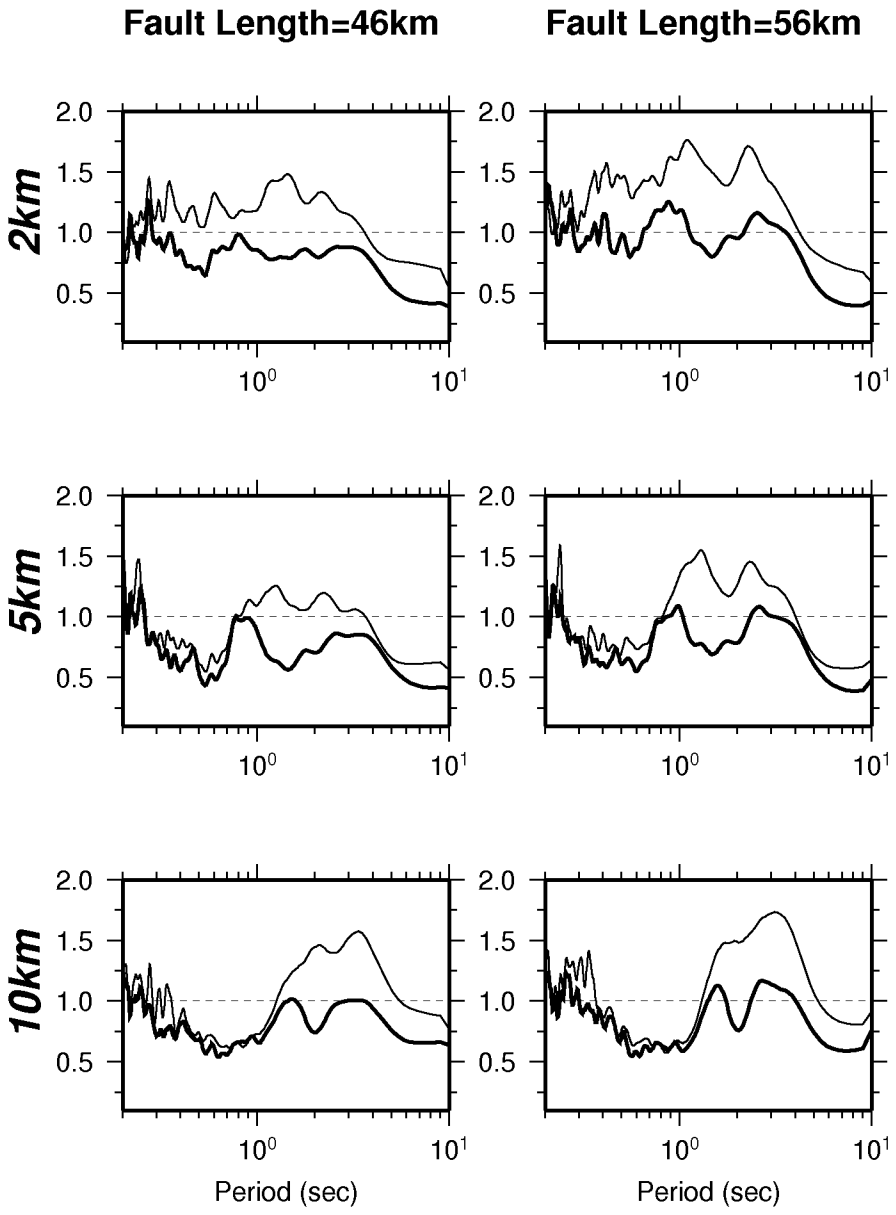

Figure 10b. Same as Figure 10a but for stations with D between 20 km and 30 km.

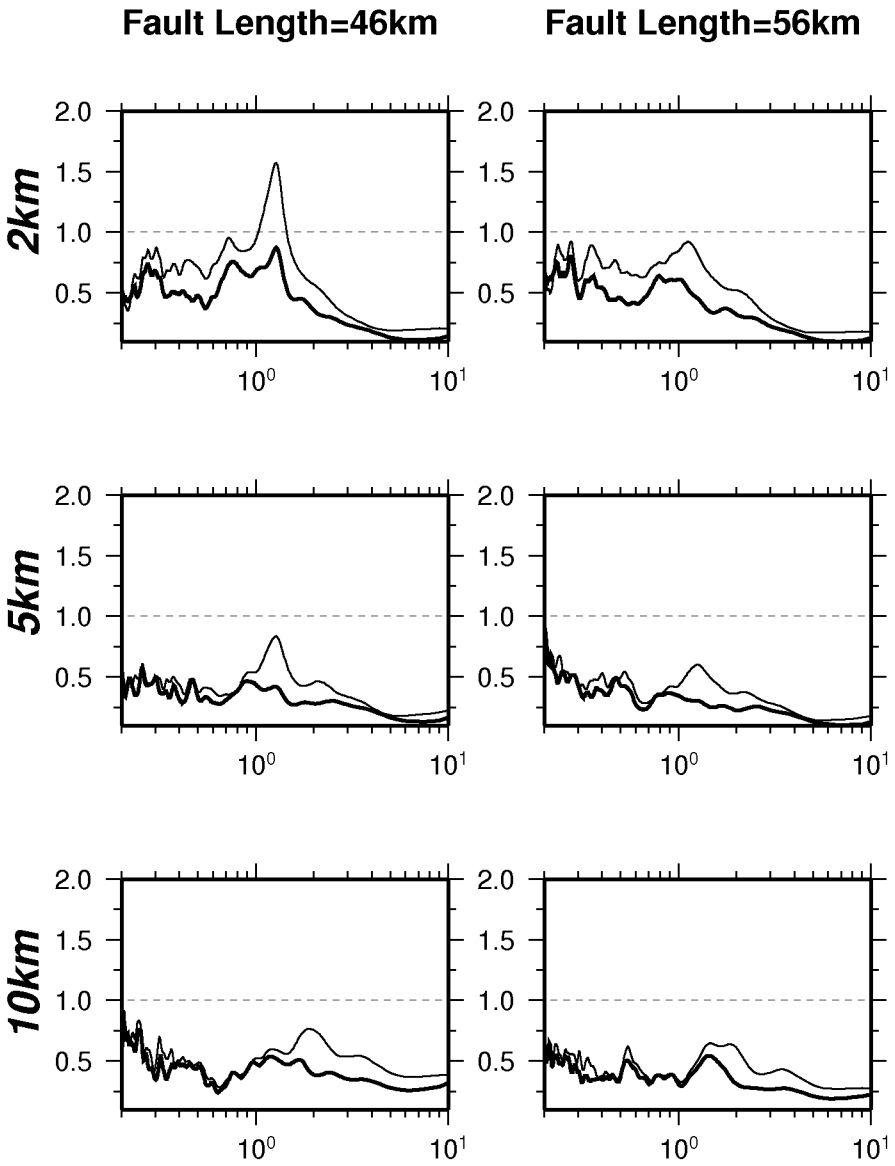

Figure 10c. Same as Figure 10a but for stations with D larger than 30 km

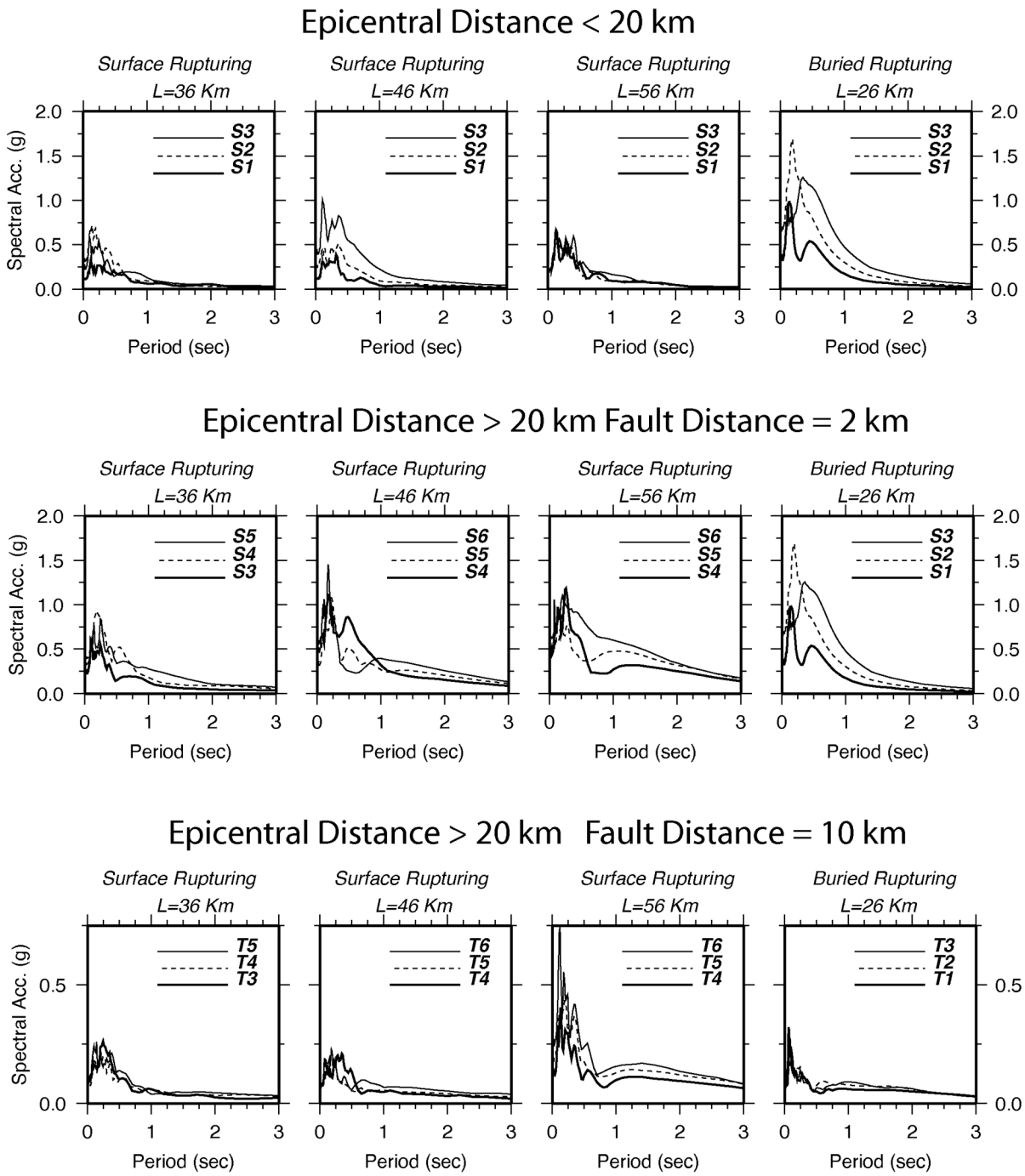

Figure 11. Fault-normal acceleration response spectra for different fault lengths and type of rupture. The spectra are calculated at selected stations with D, distance along the fault away from the epicenter, smaller than 20 km (top panels), at D larger than 20km and fault distance 2 km (middle panels), and D larger than 20 km and fault distance 10 km (bottom panels). The stations location is shown in Figure 4. Note the relatively large amplitude for buried rupture (right panels) compared to surface rupturing earthquakes with larger magnitude. The type of rupture and fault length L are indicated on top of each panel.